OPTICS

Laser vaporization of cirrus-like ice particles with secondary ice multiplication

10.1126/sciadv.1501912

Mary Matthews,[1]* François Pomel,[1] Christiane Wender,[2] Alexei Kiselev,[2] Denis Duft,[2] Jérôme Kasparian,[3] Jean-Pierre Wolf,[1] Thomas Leisner[2]

We investigate the interaction of ultrashort laser filaments with individual 90-µm ice particles, representative of cirrus particles. The ice particles fragment under laser illumination. By monitoring the evolution of the corresponding ice/vapor system at up to 140,000 frames per second over 30 ms, we conclude that a shockwave vaporization supersaturates the neighboring region relative to ice, allowing the nucleation and growth of new ice particles, supported by laser-induced plasma photochemistry. This process constitutes the first direct observation of filament-induced secondary ice multiplication, a process that strongly modifies the particle size distribution and, thus, the albedo of typical cirrus clouds.

INTRODUCTION

Cirrus clouds are ice particle clouds (*1*) that cover up to 30% of the upper troposphere (altitude, 6 to 12 km) (*2*). Their impact on the albedo, or reflectivity, of Earth is highly dependent on the shape and size distribution of the ice particles (*3*). Cirrus clouds consist of two families of ice particles, depending on the cooling rate during their formation. Slow cooling yields crystalline platelets, whereas fast cooling results in spherical, polycrystalline ice particles (*4*). To date, the interaction of ultrashort, intense laser pulses with the latter is unknown and can be expected to be very rich because these particles exhibit both the spherical shape of liquid droplets, which allows internal focusing of the incident light, and a solid-gas interface reminiscent of the interaction of light with ice surfaces in the context of, for example, laser ablation.

In the case of micrometric liquid droplets, phenomena such as Rayleigh-like jets (*5*), water film formation, bubble cavitation, and shockwaves are observed for laser intensities ~1 to 10 TW/cm^2 (*6*–*11*). The laser is focused by the curved surface of the droplet onto a hot spot that has a diameter of a few micrometers (*12*, *13*) with local intensities in the range of 10^{15} W/cm^3. This is sufficient to ionize water beyond the critical electron density (1.7×10^{21} cm^{-3} at 800 nm) (*14*). The generated plasma efficiently absorbs the whole laser energy coupled into the particle and acts as a white-light nanosource (*15*), with wide-ranging applications from atmospheric remote sensing to drug delivery (*16*). At higher incident intensities (>10 TW/cm^2), ionization occurs at the surface of the water droplet as well, which partially shields the penetration in the liquid (*17*).

The interaction of high-intensity lasers with the surface of solid ice has been extensively investigated in the context of laser ablation (*18*, *19*). During femtosecond laser interaction with the solid surface, energy is absorbed via multiphoton, tunnel, and impact ionization (*20*), with ionization rates of ~10^{15} s^{-1}. Electron and phonon relaxation occurs on a picosecond time scale, accompanied by an equivalent rapid rise in the material temperature and pressure, which is faster than thermal diffusion to neighboring regions, ~10^{-6} s. This leads to a microexplosion (that is, a shockwave emission of up to several gigapascals), ultrafast melting and vaporization, matter ejection, and subsequent resolidification.

The femtosecond irradiation of a spherical micrometric ice particle can be expected to exhibit similar features of plasma generation and shockwaves. However, the micrometric particle size affects the diffusion of heat and the propagation of shockwaves. Furthermore, the high surface-to-volume ratio strongly affects the energy balance. A fundamental question is the assessment of phase transitions, such as melting, vaporization, and sublimation during or after the interaction with the laser pulse.

Although these processes at play have already been identified in liquid droplets and/or at solid interfaces, their relative contribution and their interaction in micrometric ice particles are unclear. For example, the amount of water vaporized and the associated time scales are unknown to date, although they are critical to predicting the subsequent evolution of the air mass around the particle.

Here, on the basis of direct video recording at a rate of up to 140,000 frames per second (fps), as well as mass and energy budgets, we investigate the interaction of ultrashort, intense laser pulses with cirrus-like ice particles. The ice particle simultaneously shatters and partially evaporates, releasing water vapor until supersaturation is reached and triggers the nucleation and growth of new, smaller ice particles. Such nucleation, increasing the particle number density and decreasing their average size, constitutes the direct observation of filament-induced secondary ice multiplication (FISIM) in cirrus-like clouds (*21*), in which ultrashort laser pulses induce an up to 100-fold increase in particle density that could modify their albedo and radiative forcing properties. Furthermore, the possibility of initiating laser-induced shockwaves in ice could lead to a new method of generating gigapascal pressures for the formation of rare or superionic ice structures (*22*).

RESULTS

As displayed in Fig. 1, each individual ice particle is injected into an electrodynamic Paul trap as a distilled water droplet, using a piezo-injector. It homogeneously freezes into a 90-µm ice particle during its descent into the trap, which is kept at a temperature of −41°C (that is, below homogeneous freezing) by a copper cold finger. Two open ports (3 mm in diameter) on both sides of the trap allow the laser to

[1]Université de Genève, GAP-Biophotonics, Chemin de Pinchat 22, 1211 Geneva 4, Switzerland. [2]Karlsruhe Institute of Technology, Hermann-von-Helmholtz-Platz 1, 76344 Eggenstein-Leopoldshafen, Germany. [3]Université de Genève, GAP-Nonlinear, Chemin de Pinchat 22, 1211 Geneva 4, Switzerland.
*Corresponding author. Email: mary.matthews@unige.ch

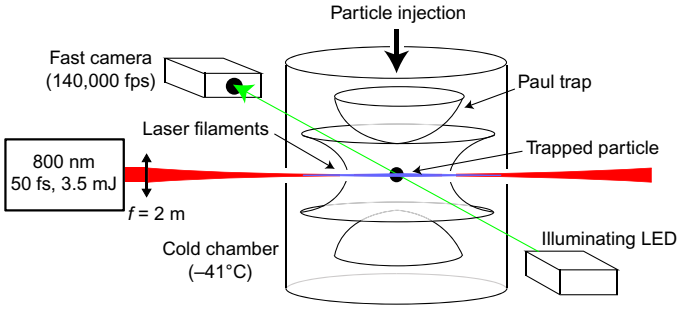

Fig. 1. Experimental setup. A single ice particle is levitated in a quadrupolar Paul trap and irradiated by a high-intensity laser filament. Particle explosion and vaporization and subsequent secondary ice formation are recorded by a digital camera at 140,000 fps.

irradiate the ice particle without interacting with windows. Because the trap is open and much colder than the ambient air, the equilibrium relative humidity with respect to ice is close to 100% in the trap center. A Ti:sapphire chirped pulse amplification laser system delivers 50-fs pulses with energies of up to 3.5 mJ at 800 nm. The laser beam is slightly focused (f = 2 m), generating an approximately 2-cm-long filament in the air through the trap center. Laser filaments (*23*–*26*) originate from a nonlinear self-guided propagation regime of high-power, ultrashort pulses. They rely on the interplay between self-focusing by the Kerr effect and defocusing caused by the ionization of the medium (here, the surrounding air), yielding a dynamic balance for intensities ~1×10^{13} to 5×10^{13} W/cm^2 (*27*) over a diameter of ~100 to 200 μm. Only a small fraction (~100 to 200 μJ) of the total laser energy is contained in the filament, with the remaining being held in a surrounding energy reservoir (*21*–*23*) of the size of the geometric waist. Because of their unique properties (extended plasma channels, high intensity inducing efficient photochemistry, coherent supercontinuum generation, self-guiding, etc.), laser filaments have been identified as attractive candidates for atmospheric sensing and for modulating atmospheric processes (*21*, *28*–*30*).

Ice particle shattering

The evolution of each ice particle after interaction with the laser is monitored at a rate of up to 140,000 fps by an ultrafast camera equipped with a microscope objective (×5) and an illuminating light-emitting diode (LED). Because of the fast cooling rate experienced by the droplet during its descent in the Paul trap, the ice particle exhibits an almost spherical, polycrystalline structure (Fig. 2) (*31*). When the laser hits the particle (t = 0), "hot spots" of scattered laser light and plasma emission are observed close to both the illuminated and shadow faces of the particle (Fig. 2, A and B). The scattering intensity distribution is different from that of a spherical liquid droplet because of the polycrystalline structure of the ice particle and surface roughness. At 2.8 mJ (Fig. 2C), the entire particle is illuminated, locally saturating the image. Because of the relatively strong focusing of the beam, the usual intensity clamping process (*27*) is not fully active, which explains the differences in plasma emission between 1.8 and 2.8 mJ.

However, the initial energy and plasma distribution within the particle does not significantly affect the fragmentation dynamics of the particle (t = 7 μs or t = 12 μs; right column of Fig. 2). Indeed, the pattern of fragmentation on the first frame after illumination is qualitatively similar for all incident laser energies and highly reproducible from one experimental realization to another. Typically, 10 to 15 fragments with a diameter of 5 μm are visible within the depth of field of the camera (Fig. 2), which can be geometrically extrapolated to a total of ~50 to 100 particles in the cone covered by the fragments. These fragments account for only a few percent of the initial mass. Simultaneously, a fragment with a diameter of 83 ± 5 μm, bearing three-quarters of the original particle mass of the particle, is ejected backward. Therefore, 10 to 15% of the initial mass is missing, indicating that it has been vaporized in the surrounding air within a few microseconds.

Nucleation of new ice particles

At later times (Fig. 3 and movie S1), more than 10 freshly grown static particles of at least several micrometers appear within the depth of field of the imaging system in the trap center (from t = 24 μs in Fig. 3 and from t = 12.1 ms in Fig. 4). In contrast to the fragments resulting from particle shattering that are ejected with momentum from the explosion, these particles have no kinetic energy and stay in the trap over times of up to milliseconds. In Fig. 4 and in movie S2, we see a few tens of new ice particles, with an average diameter of ~5 μm, periodically reilluminated by scattered light from later laser shots. These particles are visible 12 ms after the first illumination by a filament and 2 ms after a second filament. They are generated along the trajectory of the main fragment. One such static particle, located ~200 μm away from the initial position of the parent particle, was monitored over 30 ms, starting from t = 900 μs (Fig. 5). This particle starts to grow after reillumination by a second laser filament (t = 10 ms). In the early stage of its development, the particle is obviously nonspherical and spins rapidly until t = 12 ms. The second and third reilluminations (t = 20 and 30 ms, respectively) further promote particle growth, reaching a diameter of 40 μm after only 30 ms. Accordingly, the rotation slows down because of the mass increase (Fig. 5 and movie S3). The particle also reshapes while growing: after t = 17 ms, it becomes a triple-column crystal, typical of ice growth at temperatures close to 236 K (−37°C) in a supersaturated atmosphere (*32*).

DISCUSSION

Energy budget in the particle

To understand the processes at play during particle shattering and partial vaporization, and during the recondensation of new particles, we evaluated the mass and energy budget associated with the different relaxation steps and processes: plasma generation and heating, shock-wave formation, fragmentation and ejection of fragments, radiative emission, melting, and vaporization leading to supersaturation in the surrounding air. We estimated the energy deposited in the hot plasma by considering an incident intensity of ~5×10^{13} W/cm^2 [representative of a laser filament (*25*–*27*)] on the 90-μm particle and a coupling efficiency of ~50% based on Snell's law with an internal refractive index of n_{ice} = 1.31. The internal focusing of the light via spherical interface of the particle ensures efficient multiphoton, tunnel, and impact ionization at the internal focus; leads to the critical electron density (1.7×10^{21} cm^{-3}) (*14*) within the first few femtoseconds of the pulse; and results in a local opaque plasma that absorbs about 95% of the incident energy (*9*, *10*). As a result, ~100 μJ is deposited at the plasma hot spot, leading to particle fragmentation.

Tracking the position of each fragment ejected during particle shattering over several successive images for 152 fragments over 25 experimental realizations yields an average ejection speed of 5 ± 3 m/s (fig. S1), with

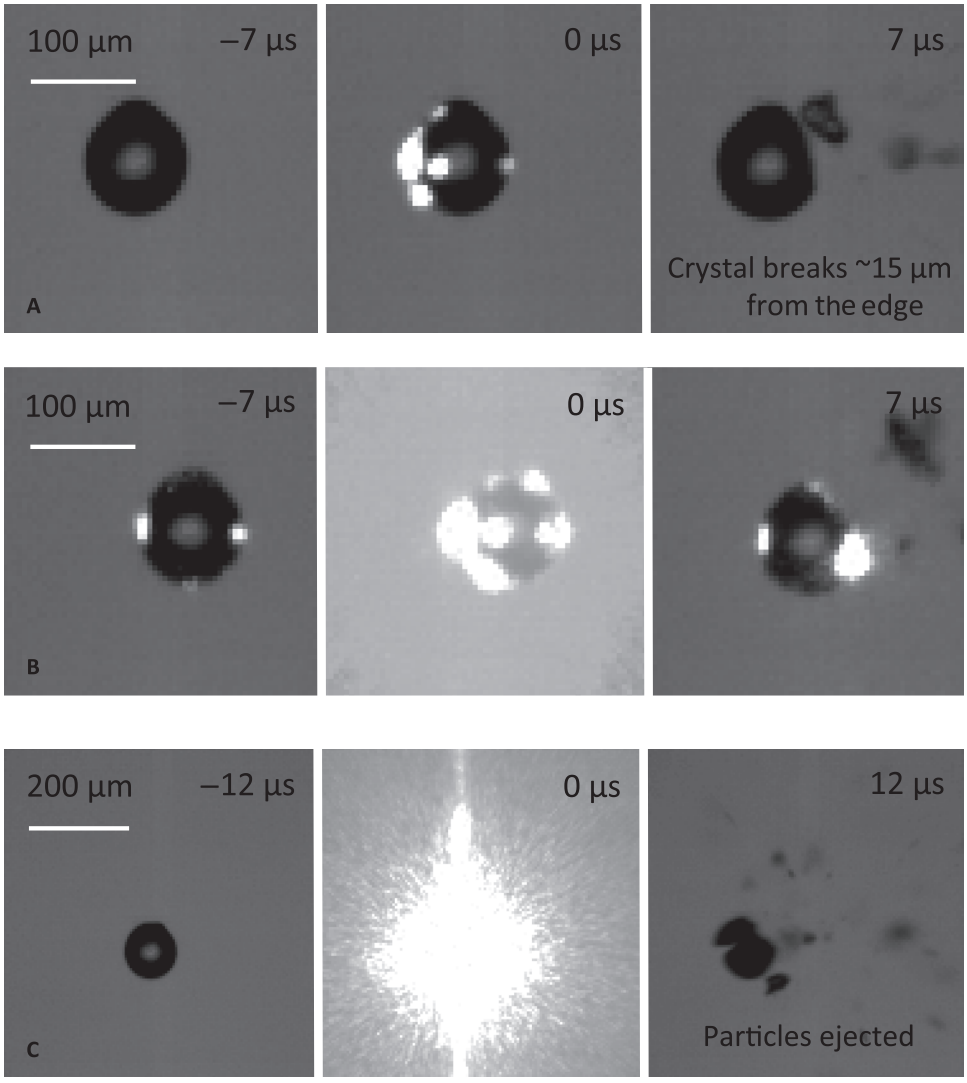

Fig. 2. Laser-induced droplet explosion. (**A** to **C**) The laser energy is (A) 1.8 mJ, (B) 2.3 mJ, and (C) 2.8 mJ. At $t = 0$ µs, scattered laser and white light from the plasma hot spots are visible, as expected for a transparent sphere. Fragmentation is visible in the last frame of each sequence.

no significant dependence on the incident laser energy. This speed corresponds to an average kinetic energy of 1 pJ per particle. Simultaneously, the main fragment is kicked backward by the explosion at a speed of 5 ± 2 m/s, corresponding to a typical kinetic energy in the 5-nJ range, again independent from the incident energy. The total kinetic energy of the system (parent particle and 100 fragments) is therefore negligible as compared to the total deposited energy of 100 µJ.

Similarly, the cohesive fracture energy of ice lies in the electron volt range per molecule (*33*). As a consequence, the cleaving and fracturing of the ice particle require energy in the nanojoule range and is negligible. The laser energy deposited in the particle is therefore almost fully available for the generation of an internal shockwave resulting in heating, melting, and vaporizing water (*9*–*11*). Stationary dissipation occurs on the millisecond time scale due to the low thermal conductivity of ice (0.024 W/cm K at 250 K) (*34*). For example, 3 ms is required for 100 µJ to spread over 2% of the particle volume. This is much too slow to account for the observed particle shattering and partial vaporization over ~10 µs. Therefore, the energy transfer has to occur through a much faster process, namely, a shockwave.

Shockwave-induced vaporization

To estimate the pressure P_0 within the shockwave and the velocity v_0 of its wavefront, we can first rely on the hydrodynamics equations (*35*, *36*) $E_0 = P_0 V_0$ and $v_0 = (P_0/\rho_0)^{1/2}$, where $E_0 = 100$ µJ is the initial energy stored in a plasma volume V_0 and ρ_0 is the density of ice. Because of the internal focusing properties of the spherical particle, the initial electronically hot plasma (ions do not move over the 50-fs time scale of the laser excitation) is localized in a cylindrical volume with a radius of ~5 µm [calculated and measured by pump-probe diffraction on droplets (*5*)] and a length of ~10 µm (*6*). This leads to a V_0 of ~800 µm^3, a velocity of the shockfront of ~10^4 m/s, and a shockwave pressure, P_0, of ~120 GPa. Such pressure is significantly larger than that observed in the case of laser-induced shockwaves in bulk water (<30 GPa) (*9*, *37*–*39*) and is due to the tight internal focusing effect in spherical particles. Indeed, pressures on the order of

terapascals have been measured for shockwaves in sapphire using very tight focusing (*26*).

A shockwave of this magnitude will likely partially vaporize ice particles through pressure-induced vaporization, similar to that observed in microexplosions in other solids (*33*, *40*). This has been reported in ice, in meteor collisions on ice surfaces (*41*), and in recent laboratory measurements, where a Hugoniot shock led to incipient melting at pressures greater than 0.6 GPa and complete melting at pressures greater than 2.5 GPa (*40*, *42*–*44*).

The moving pressure front leads to heating (*9*, *43*, *45*, *46*) of the ice particle at the nanosecond time scale. The radius R of the region swept by the shockwave can be estimated as a function of the shockwave energy E_0 (*14*): $R = (3E_0/4\pi Y)^{1/3}$ where Y is Young's elastic modulus for ice [between 1 and 9 GPa (*47*)]. That is, the energy E_0 required to produce a shockwave over a volume V_0 is $E_0 = V_0 Y$. As the energy absorbed in the hot spot is 100 μJ, a distance between 13 and 28 μm is swept by the shockwave before it becomes a sound wave. The corresponding volume covers 2 to 24% of the particle. Such volume is likely to experience ultrafast

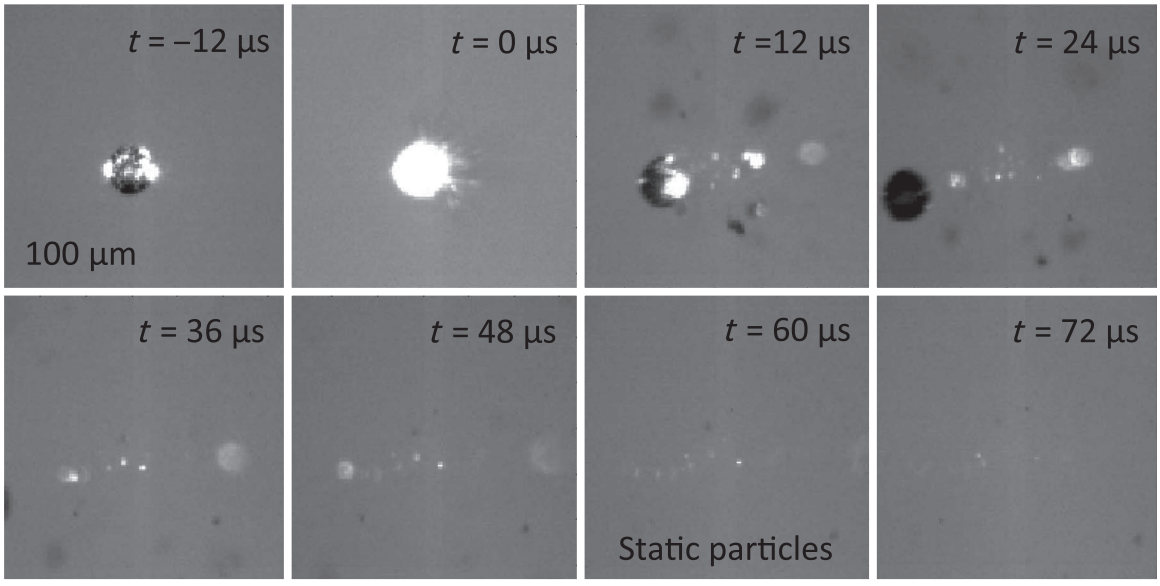

Fig. 3. Formation of new ice particles. This formation follows the explosion of an ice particle induced by a single incident laser pulse of 50-fs duration and an energy of 3.5 mJ. The frame interval is 12 μs, and the exposure time is 1 μs. The full sequence is available as movie S1.

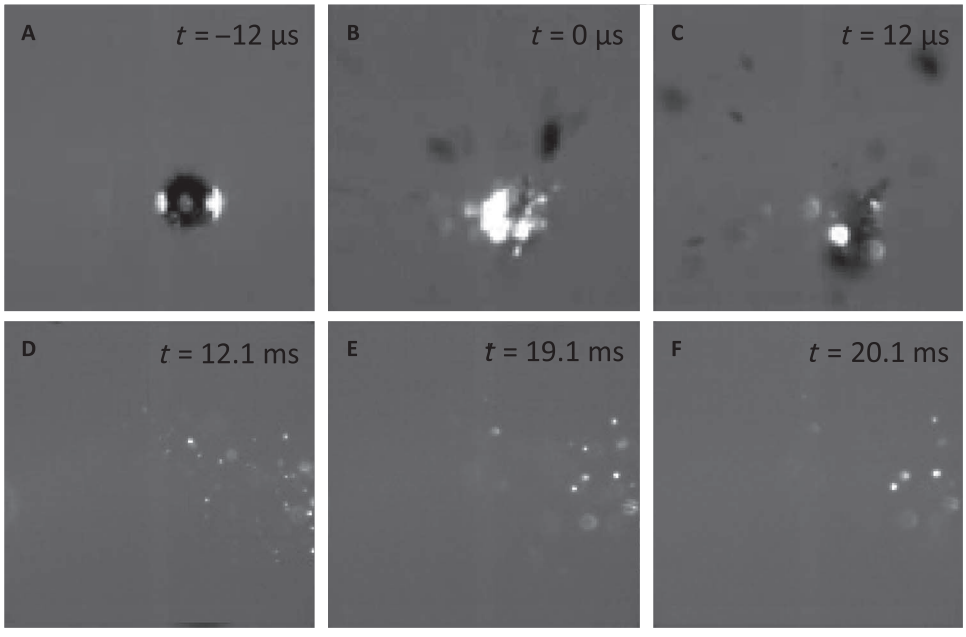

Fig. 4. Formation of new, homogeneously frozen ice particles. It follows the explosion of an ice particle. (**A**) Particle before the laser illumination. (**B**) Laser illumination. (**C**) Particle explosion. The main fragment is ejected backward and leaves the field of view, whereas many smaller particles are ejected from the shadow face. (**D** to **F**) Formation of smaller particles along the trajectory of the larger fragment after further illuminations by the laser filament. See movie S2.

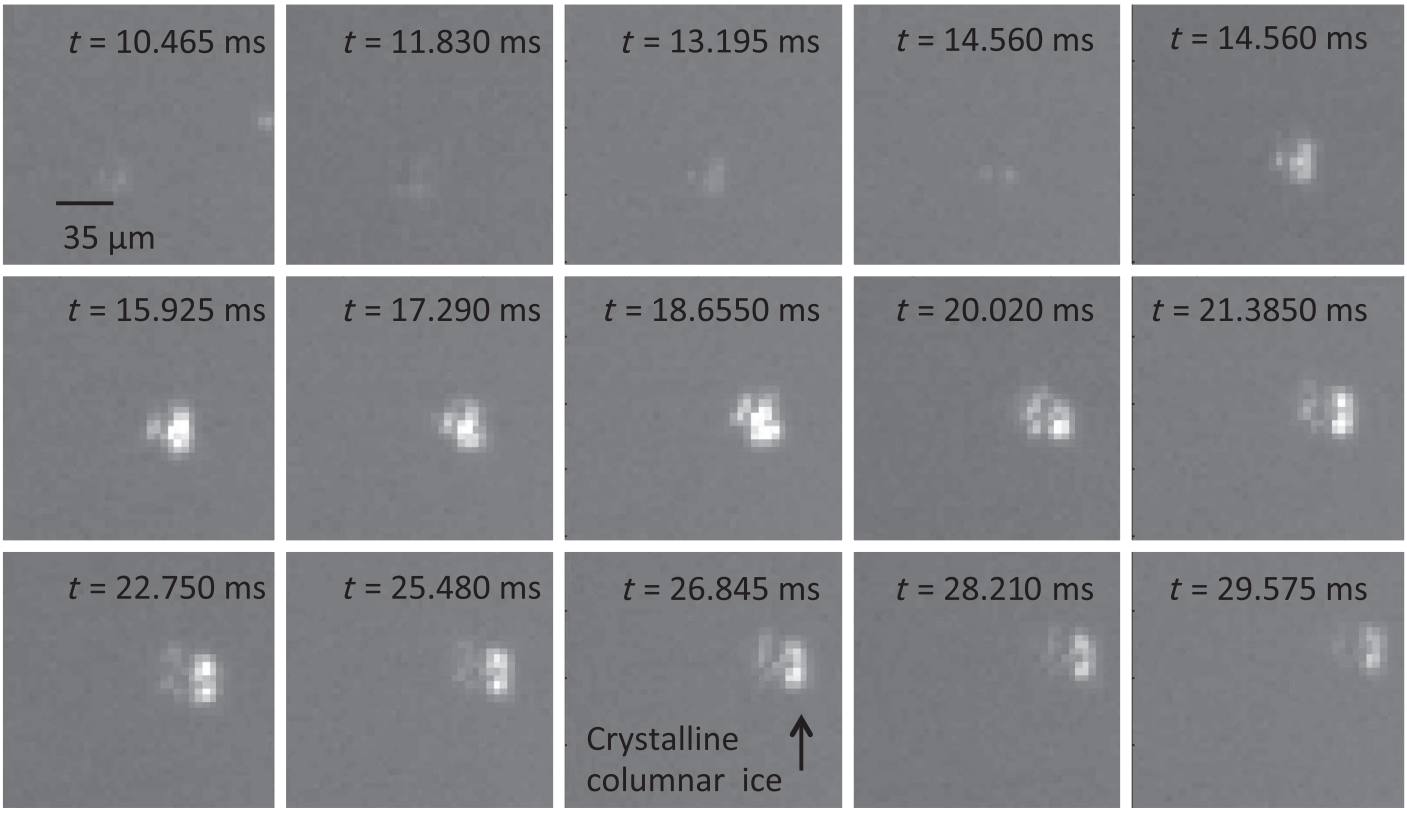

Fig. 5. Growth of a stable particle. The particle has an initial diameter of 18 µm, 200 µm away from the initial particle position. After a reillumination at t = 10 ms, it grows up to 40 µm, with a progressive change in structure. At t = 26 µs, it takes the form of a triple ice rod. Simultaneously, a smaller particle evaporates. The full sequence is available as movie S3.

heating from the laser-induced shockwave. This vaporized fraction is consistent with the analysis of the high-speed video frames (Figs. 2 and 3): the laser reduces the diameter of the parent particle by 8% on average, corresponding to 20% of the initial particle volume ablated on the shadow side of the particle. On the other hand, the already mentioned 100 fragments with a diameter of 5 µm account for a few percent of the volume of the initial 90-µm-diameter particle. Therefore, 10 to 15% of the parent ice particle mass is available for vaporization.

Local supersaturation and new particle formation

A vaporization of 10 to 15% of the initial particle mass is also consistent with the energy budget of the process. Consider a typical value for the specific heats of ice and water (2.11 and 4.2 J/g K, respectively) and latent heat of fusion (334 J/g) and vaporization (2260 J/g). The specific energy required to vaporize ice from an initial temperature of −41°C amounts to 3100 J/g. The available 100 µJ can therefore vaporize 30 ng of water, 10% of the 300 ng of the parent particle, which is again consistent with the 2 to 24% obtained based on the volume swept by the shockwave radius. Because the internal energy of water is a state function, the pathway followed for vaporization (for example, melting followed by vaporization or sublimation) does not influence the energy balance.

Such release of substantial amounts of water into the gas phase around the particle induces supersaturation in the center of the trap, which is a key ingredient that allows the nucleation of new particles. Because the trap is in a thermodynamically stable regime before the particle is introduced, its relative humidity with regard to ice cannot exceed saturation, that is, 3.5×10^{15} molecules/cm^3 (9×10^{-8} g/cm^3) at −41°C. Even with the assumption that all water molecules available inside a volume of 1 mm^3 would condense, they would only form a single particle of only a few micrometers in diameter, much less than what is actually observed (40 µm after 30 ms; see Fig. 5 and movie S3). Furthermore, diffusion of water from the laboratory (T = 20°C, relative humidity = 40%) to the center of the trap through the open ports would have a time constant on the order of 1 min, which is much slower than the microsecond to millisecond time scale of the observed ice particle growth. Therefore, significant particle nucleation cannot occur without the supply of water vapor from the initial ice particle.

Evaporating 5×10^4 µm^3 (10%) from the parent ice particle corresponds to 1.5×10^{15} molecules, which can induce saturation (S = 1) in the air surrounding the particle over 1 cm^3, or S_{Ion} = 4 over 250 mm^3, or S_{Homo} = 15 over 66 mm^3 (*21*, *48*). These values of supersaturation correspond to the thresholds of ion-induced nucleation and homogeneous nucleation, respectively (*21*). Such large, highly supersaturated volume that is associated with the products of the plasma photochemistry initiated by the laser pulse allows the massive nucleation and growth of new particles (*28*, *29*, *49*, *50*). This process was previously proposed for interpreting results observed in a large cloud chamber and named filament-induced secondary ice multiplication (FISIM) (*21*).

Growth of new ice particles

The speedup of particle growth by laser reilluminations can be understood by considering the laser action on the atmosphere that is due to

not only the filaments but also the energy reservoir, that is, the fraction of the laser power that is not guided into the filaments (*51*). At the time of reilluminations ($t \geq 10$ ms), no particle is directly hit by the laser filament: the fragments can be as far as several millimeters away from the beam axis, whereas the growing particle is offset by 300 μm from the trap center. They are therefore hit by the moderate-intensity photon bath (<1 GW/cm^2) rather than by the filament itself, preventing any shattering of either the growing particle or previous fragments.

On the other hand, the photon reservoir is sufficiently intense to activate the plasma photochemistry typical of laser-induced condensation and particle growth (*21*, *27*–*29*, *49*, *50*). It therefore releases condensable and/or hygroscopic species such as ozone, nitrogen oxides, •OH radicals, or oxidized organics close to the growing particle. The high concentration of these species (*52*) allows very fast growth rates observed in the image sequence in Fig. 5, yielding particles of some tens of micrometers within milliseconds, in line with previous observations and modeling of laser-induced particles (*28*, *29*).

Thus, we expect that the formation of new particles occurs in two steps. The high local supersaturation first allows a rapid nucleation of water vapor, below −37°C. This nucleation is assisted by the filament plasma products generated in the very vicinity of the particle. Subsequently, the particles freeze homogeneously and survive as the temperature stays below −37°C. The laser might also contribute to particle growth by increasing the diffusion of water vapor and particle coalescence due to the convection and the thermal shockwave that is also generated in air by the filaments (*53*, *54*).

CONCLUSION

As a conclusion, we have observed the effect of laser filaments illuminating individual 100-μm ice particles, as well as the subsequent evolution of the interaction region, over up to 30 ms. Internal focusing of the incident light produces a plasma hot spot that absorbs almost the whole incident laser energy. The resulting shockwave partially vaporizes the ice. This partial vaporization induces strong local supersaturation relative to ice in the surrounding air, allowing the nucleation of particles in the trap center (*21*). Supported by laser plasma photochemistry triggered by the subsequent laser pulses, these newly nucleated particles grow up to 40 μm. This process drastically affects the cloud size distribution, with an increase in the particle number density together with a decrease in their average size. This process is associated with a net increase in the total mass of condensed water, as observed in FISIM (*21*). Besides providing a description of laser interaction with a system that shares properties with spherical liquid droplets and air-ice interfaces, our results open prospects to modifying the particle size distribution and, thus, the albedo of cirrus ice particle clouds.

MATERIALS AND METHODS

As shown in Fig. 1, the experiment relied on a piezoelectric injector that launched negatively charged, distilled water droplets of ~90-μm diameter into a Paul trap kept at a temperature of −41°C by a copper cold finger. The temperatures of the air in the trap and in the copper cold finger were measured with two platinum thermocouples. As detailed elsewhere (*55*, *56*), the trap consisted of three hyperbolic electrodes, through which ac and dc electric fields were applied to create a saddle-shaped electromagnetic potential. The water was injected from the top as a liquid droplet that froze homogeneously during the 80 ms of its descent into the trap. Because the trap was open and much colder than the ambient air, the equilibrium relative humidity in the trap center was close to 100% with respect to ice. The particles were illuminated by a laser diode. Their Mie scattering pattern was observed by a two-dimensional charge-coupled device (CCD) to determine the size of spherical particles or to assess its nonsphericity. On the same port, a beam splitter sampled a fraction of the particle scattering on a CCD line array to measure the height of the particle within the trap and provided feedback to adjust the voltage to the dc electrodes and stabilize the height of the droplet within the trap. Two open ports (3 mm in diameter) on both sides of the trap allowed the laser to hit the particles in its center. A Ti:sapphire chirped pulse amplification system delivered 50-fs pulses with an energy of up to 3.5 mJ at a wavelength of 800 nm. This beam was focused (f = 2 m) into a 2-mm-diameter beam waist, generating a self-guided filament in the trap center.

The video recording system used an ultrafast camera (Phantom v.7.3, up to 200,000 fps, 600 × 800 pixels, 22 μm × 22 μm each) through a ×5 imaging system, with a field of view of 2.64 mm, a resolution of 4.5 μm/pixel (allowing the observation of particles that were 2 μm or larger), and a depth of field of 8 μm. The particles were back-illuminated by an LED, in a Kohler arrangement (*57*). The viewing angle was 45° from the laser direction. To fulfill the Scheimpflug condition (*58*) and provide a sharp image along the beam axis, the camera image plane was tilted accordingly.

SUPPLEMENTARY MATERIALS

Supplementary material for this article is available at http://advances.sciencemag.org/cgi/content/full/2/5/e1501912/DC1

movie S1. Explosion of an ice particle illuminated with a high-intensity laser.
movie S2. Formation of new ice particles.
movie S3. Growth of an ice particle nucleated in the Paul trap.
fig. S1. Probability distribution function of the ejection speeds of the fragments.

REFERENCES AND NOTES

1. P. H. Wang, P. Minnis, M. P. McCormick, G. S. Kent, K. M. Skeens, A 6-year climatology of cloud occurrence frequency from stratospheric aerosol and gas experiment II observations (1985–1990). *J. Geophys. Res.* **101**, 29407–29429 (1996).
2. F. Franks, Nucleation of ice and its management in ecosystems. *Philos. Trans. R. Soc. London Ser. A* **361**, 557–574 (2003).
3. K.-N. Liou, Influence of cirrus clouds on weather and climate processes: A global perspective. *Mon. Weather Rev.* **114**, 1167–1199 (1986).
4. J. H. Seinfeld, S. N. Pandis, *Atmospheric Chemistry and Physics—From Air Pollution to Climate Change* (Wiley, Hoboken, NJ, ed. 2, 2006).
5. D. Duft, T. Achtzehn, R. Müller, B. A. Huber, T. Leisner, Coulomb fission: Rayleigh jets from levitated microdroplets. *Nature* **421**, 128 (2003).
6. A. Lindinger, J. Hagen, L. D. Socaciu, T. M. Bernhardt, L. Wöste, D. Duft, T. Leisner, Time-resolved explosion dynamics of H_2O droplets induced by femtosecond laser pulses. *Appl. Optics* **43**, 5263–5269 (2004).
7. S. T. Thoroddsen, K. Takehara, T. G. Etoh, C.-D. Ohl, Spray and microjets produced by focusing a laser pulse into a hemispherical drop, *Phys. Fluids* **21**, 112101 (2009).
8. E. S. Efimenko, Y. A. Malkov, A. A. Murzanev, A. N. Stepanov, Femtosecond laser pulse-induced breakdown of a single water microdroplet. *J. Opt. Soc. Am. B* **31**, 534–541 (2014).
9. B. D. Strycker, M. M. Springer, A. J. Traverso, A. A. Kolomenskii, G. W. Kattawar, A. V. Sokolov, Femtosecond-laser-induced shockwaves in water generated at an air-water interface. *Opt. Express* **21**, 23772–23784 (2013).
10. F. V. Potemkin, E. I. Mareev, A. A. Podshivalov, V. M. Gordienko, Laser control of filament-induced shock wave in water. *Laser Phys. Lett.* **11**, 106001 (2014).
11. F. V. Potemkin, E. I. Mareev, A. A. Podshivalov, V. M. Gordienko, Highly extended high density filaments in tight focusing geometry in water: From femtoseconds to microseconds. *New J. Phys.* **17**, 053010 (2015).

12. F. Courvoisier, V. Boutou, C. Favre, S. C. Hill, J.-P. Wolf, Plasma formation dynamics within a water microdroplet on femtosecond time scales. *Opt. Lett.* **28**, 206–208 (2003).
13. V. Boutou, C. Favre, S. C. Hill, Y. L. Pan, R. K. Chang, J. P. Wolf, Backward enhanced emission from multiphoton processes in aerosols. *Appl. Phys. B* **75**, 145–152 (2002).
14. W. Theobald, R. Häßner, R. Kingham, R. Sauerbrey, R. Fehr, D. O. Gericke, M. Schlanges, W.-D. Kraeft, K. Ishikawa, Electron densities, temperatures, and the dielectric function of femtosecond-laser-produced plasmas. *Phys. Rev. E* **59**, 3544 (1999).
15. C. Favre, V. Boutou, S. C. Hill, W. Zimmer, M. Krenz, H. Lambrecht, J. Yu, R. K. Chang, L. Woeste, J.-P. Wolf, White-light nanosource with directional emission. *Phys. Rev. Lett.* **89**, 035002 (2002).
16. G. Lajoinie, E. Gelderblom, C. Chlon, M. Böhmer, W. Steenbergen, N. de Jong, M. Versluis, Ultrafast vapourization dynamics of laser-activated polymeric microcapsules. *Nat. Commun.* **5**, 3671 (2014).
17. C. Jeon, D. Harper, K. Lim, M. Durand, M. Chini, M. Baudelet, M. Richardson, Interaction of a single laser filament with a single water droplet. *J. Opt.* **17**, 055502 (2015).
18. R. R. Gattass, E. Mazur, Femtosecond laser micromachining in transparent materials. *Nat. Photonics* **2**, 219–225 (2008).
19. S. S. Mao, F. Quéré, S. Guizard, X. Mao, R. E. Russo, G. Petite, P. Martin, Dynamics of femtosecond laser interactions with dielectrics. *Appl. Phys. A* **79**, 1695–1709 (2004).
20. L. V. Keldysh, Ionization in the field of a strong electromagnetic wave. *Sov. Phys. JETP* **20**, 1307–1314 (1965).
21. T. Leisner, D. Duft, O. Möhler, H. Saathoff, M. Schnaiter, S. Henin, K. Stelmaszczyk, M. Petrarca, R. Delagrange, Z. Hao, J. Lüder, Y. Petit, P. Rohwetter, J. Kasparian, J.-P. Wolf, L. Wöste, Laser-induced plasma cloud interaction and ice multiplication under cirrus cloud conditions. *Proc. Natl. Acad. Sci. U.S.A.* **110**, 10106–10110 (2013).
22. J. Sun, B. K. Clark, S. Torquato, R. Car, The phase diagram of high-pressure superionic ice. *Nat. Commun.* **6**, 8156 (2015).
23. J. Kasparian, M. Rodriguez, G. Méjean, J. Yu, E. Salmon, H. Wille, R. Bourayou, S. Frey, Y.-B. André, A. Mysyrowicz, R. Sauerbrey, J.-P. Wolf, L. Wöste, White-light filaments for atmospheric analysis. *Science* **301**, 61–64 (2003).
24. A. Couairon, A. Mysyrowicz, Femtosecond filamentation in transparent media. *Phys. Rep.* **44**, 47–189 (2007).
25. L. Bergé, S. Skupin, R. Nuter, J. Kasparian, J.-P. Wolf, Ultrashort filaments of light in weakly-ionized, optically-transparent media. *Rep. Prog. Phys.* **70**, 1633 (2007).
26. J. Kasparian, J.-P. Wolf, Physics and applications of atmospheric nonlinear optics and filamentation. *Opt. Express* **16**, 466–493 (2008).
27. J. Kasparian, R. Sauerbrey, S. L. Chin, The critical laser intensity of self-guided light filaments in air. *Appl. Phys. B* **71**, 877–879 (2000).
28. P. Rohwetter, J. Kasparian, K. Stelmaszczyk, Z. Hao, S. Henin, N. Lascoux, W. M. Nakaema, Y. Petit, M. Queißer, R. Salamé, E. Salmon, L. Wöste, J.-P. Wolf, Laser-induced water condensation in air. *Nat. Photonics* **4**, 451–456 (2010).
29. S. Henin, Y. Petit, P. Rohwetter, K. Stelmaszczyk, Z. Q. Hao, W. M. Nakaema, A. Vogel, T. Pohl, F. Schneider, J. Kasparian, K. Weber, L. Wöste, J.-P. Wolf, Field measurements suggest the mechanism of laser-assisted water condensation. *Nat. Commun.* **2**, 456 (2011).
30. D. Mongin, J. G. Slowik, E. Schubert, J.-G. Brisset, N. Berti, M. Moret, A. S. H. Prévôt, U. Baltensperger, J. Kasparian, J.-P. Wolf, Non-linear photochemical pathways in laser-induced atmospheric aerosol formation. *Sci. Rep.* **5**, 14978 (2015).
31. B. Krämer, O. Hübner, H. Vortisch, L. Wöste, T. Leisner, M. Schwell, E. Rühl, H. Baumgärtel, Homogeneous nucleation rates of supercooled water measured in single levitated microdroplets. *J. Chem. Phys.* **111**, 6521–6527 (1999).
32. M. Bailey, J. Hallett, Growth rates and habits of ice crystals between −20° and −70°C. *J. Atmos. Sci.* **61**, 514–544 (2004).
33. A. Stuart, Rice, A. R. Dinner, *Advances in Chemical Physics* (Wiley, New York, 2011), vol. 147.
34. G. A. Slack, Thermal conductivity of ice. *Phys. Rev. B* **22**, 3065 (1980).
35. E. G. Gamaly, S. Juodkazis, K. Nishimura, H. Misawa, B. Luther-Davies, L. Hallo, P. Nicolai, V. T. Tikhonchuk, Laser-matter interaction in the bulk of a transparent solid: Confined microexplosion and void formation. *Phys. Rev. B* **73**, 214101 (2006).
36. S. Juodkazis, K. Nishimura, S. Tanaka, H. Misawa, E. G. Gamaly, B. Luther-Davies, L. Hallo, P. Nicolai, V. T. Tikhonchuk, Laser-induced microexplosion confined in the bulk of a sapphire crystal: Evidence of multimegabar pressures. *Phys. Rev. Lett.* **96**, 166101 (2006).
37. T. Pezeril, G. Saini, D. Veysset, S. Kooi, P. Fidkowski, R. Radovitzky, K. A. Nelson, Direct visualization of laser-driven focusing shock waves. *Phys. Rev. Lett.* **106**, 214503 (2011).
38. J. Noack, D. X. Hammer, G. D. Noojin, B. A. Rockwell, A. Vogel, Influence of pulse duration on mechanical effects after laser-induced breakdown in water. *J. Appl. Phys.* **83**, 7488–7495 (1998).
39. C. B. Schaffer, N. Nishimura, E. N. Glezer, A. M.-T. Kim, E. Mazur, Dynamics of femtosecond laser-induced breakdown in water from femtoseconds to microseconds. *Opt. Express* **10**, 196–203 (2002).
40. S.-N. Luo, T. J. Ahrens, Shock-induced superheating and melting curves of geophysically important minerals. *Phys. Earth Planet. In.* **143–144**, 369–386 (2004).
41. F. Nimmo, D. G. Korycansky, Impact-driven ice loss in outer Solar System satellites: Consequences for the Late Heavy Bombardment. *Icarus* **219**, 508–510 (2012).
42. S. T. Stewart, T. J. Ahrens, Shock properties of H_2O ice. *J. Geophys. Res.* **110**, E03005 (2005).
43. S. T. Stewart, A. Seifter, A. W. Obst, Shocked H_2O ice: Thermal emission measurements and the criteria for phase changes during impact events. *Geophys. Res. Lett.* **35**, L23203 (2008).
44. N. Goldman, E. J. Reed, I.-F. W. Kuo, L. E. Fried, C. J. Mundy, A. Curioni, Ab initio simulation of the equation of state and kinetics of shocked water. *J. Chem. Phys.* **130**, 124517 (2009).
45. D. von der Linde, K. Sokolowski-Tinten, The physical mechanisms of short-pulse laser ablation. *Appl. Surf. Sci.* **154–155**, 1–10 (2000).
46. P. Stampfli, K. H. Bennemann, Theory for the instability of the diamond structure of Si, Ge, and C induced by a dense electron-hole plasma. *Phys. Rev. B* **42**, 7163 (1990).
47. J. Noack, A. Vogel, Laser-induced plasma formation in water at nanosecond to femtosecond time scales: Calculation of thresholds, absorption coefficients, and energy density. *IEEE J. Quantum Electron.* **35**, 1156–1167 (1999).
48. D. M. Murphy, T. Koop, Review of the vapour pressures of ice and supercooled water for atmospheric applications. *Q. J. R. Meteorol. Soc.* **131**, 1539–1565 (2005).
49. P. Rohwetter, J. Kasparian, L. Wöste, J.-P. Wolf, Modelling of HNO_3-mediated laser-induced condensation: A parametric study. *J. Chem. Phys.* **135**, 134703 (2011).
50. M. Matthews, S. Henin, F. Pomel, F. Théberge, P. Lassonde, J.-F. Daigle, J.-C. Kieffer, J. Kasparian, J.-P. Wolf, Cooperative effect of ultraviolet and near-infrared beams in laser-induced condensation. *Appl. Phys. Lett.* **103**, 264103 (2013).
51. M. Petrarca, S. Henin, K. Stelmaszczyk, S. Bock, S. Kraft, U. Schramm, C. Vaneph, A. Vogel, J. Kasparian, R. Sauerbrey, K. Weber, L. Wöste, J.-P. Wolf, Multijoule scaling of laser-induced condensation in air. *Appl. Phys. Lett.* **99**, 141103 (2011).
52. Y. Petit, S. Henin, J. Kasparian, J.-P. Wolf, Production of ozone and nitrogen oxides by laser filamentation. *Appl. Phys. Lett.* **97**, 021108 (2010).
53. J. Ju, J. Liu, C. Wang, H. Sun, W. Wang, X. Ge, C. Li, S. L. Chin, R. Li, Z. Z. Xu, Laser-filamentation-induced condensation and snow formation in a cloud chamber. *Opt. Lett.* **37**, 1214–1216 (2012).
54. N. Jhajj, E. W. Rosenthal, R. Birnbaum, J. K. Wahlstrand, H. M. Milchberg, Demonstration of long-lived high-power optical waveguides in air. *Phys. Rev. X* **4**, 011027 (2014).
55. N. Hoffmann, A. Kiselev, D. Rzesanke, D. Duft, T. Leisner, Experimental quantification of contact freezing in an electrodynamic balance. *Atmos. Meas. Tech.* **6**, 2373–2382 (2013).
56. T. Leisner, Laboratory experiments on single levitated aerosol particles, in *Progress in Experimental and Theoretical Studies of Clusters*, T. Kondow, F. Mafune, Eds. (World Scientific Publishing, Singapore, 2003), pp. 239–260.
57. A. Koehler, New method of illumination for photomicrographical purposes. *J. R. Microscopical Soc.* **14**, 261–262 (1894).
58. A. K. Khurana, *Theory and Practice of Optics and Refraction* (Elsevier India, New Delhi, India, ed. 2, 2008).

Acknowledgments: We acknowledge C. Heiman for help in the data analysis, S. Hermelin for assistance, and M. Moret for technical support. **Funding:** This work was supported by the ERC (European Research Council) advanced grant "Filatmo" and the Deutsche Forschungsgemeinschaft. We also acknowledge support from the NCCR (National Center of Competence in Research) "MUST" (Molecular Ultrafast Science and Technology) from the Swiss NSF. M.M. acknowledges the support of Marie Heim-Vogtlin grant no. S17982. **Author contributions:** J.-P.W., T.L., and J.K. conceived the experiment. D.D. and A.K. prepared and configured the Paul trap. M.M., F.P., and C.W. performed the experiment. M.M. and J.K. analyzed images and modeled the ice-laser system. M.M., J.K., and J.-P.W. wrote the paper. All authors reviewed the manuscript text. **Competing interests:** The authors declare that they have no competing interests. **Data and materials availability:** All data needed to evaluate the conclusions in the paper are present in the paper and/or the Supplementary Materials. Additional data related to this paper may be requested from the authors.

Submitted 29 December 2015
Accepted 20 April 2016
Published 20 May 2016
10.1126/sciadv.1501912

Citation: M. Matthews, F. Pomel, C. Wender, A. Kiselev, D. Duft, J. Kasparian, J.-P. Wolf, T. Leisner, Laser vaporization of cirrus-like ice particles with secondary ice multiplication. *Sci. Adv.* **2**, e1501912 (2016).

Laser vaporization of cirrus-like ice particles with secondary ice multiplication

Mary Matthews, François Pomel, Christiane Wender, Alexei Kiselev, Denis Duft, Jérôme Kasparian, Jean-Pierre Wolf and Thomas Leisner

Sci Adv **2** (5), e1501912.
DOI: 10.1126/sciadv.1501912